J. of Marine Env. Eng., Vol. 16, pp. 1–18
Reprints available directly from the publisher
Photocopying permitted by license only

Far-field Evaluation of a Lagrangian Artificial Upwelling Concept

GÉRARD C. NIHOUS[a]

Hawaii Natural Energy Institute, University of Hawaii, 1680 East-West Road, POST 109, Honolulu, Hawaii 96822, USA

The evolution of releases of deep nutrient-rich seawater near the ocean surface is examined in the absence of ambient currents once buoyancy forces vanish (far field). The proposed model extends plume calculations (near field) into a spatial and temporal framework where slow diffusive and biological processes become important. As anticipated, large releases with $Q^* \approx 100$ m^3/s fail to produce biological enhancement because of excessive depths. For moderate releases, phytoplankton and zooplankton growth would be promoted within a narrow vertical layer extending up to a few kilometers radially. Smaller plumes with $Q^* \approx 1$ m^3/s and shallower settling depths correspond to a complete far-field conversion of excess nutrients into organic matter. With moderate plumes, i.e. $Q^* \approx 10$ m^3/s and deeper neutral-buoyancy depths, photosynthesis is less efficient in processing the larger amount of excess nutrients; grazing pressure also becomes relatively stronger. Changes in the concentrations of microorganisms are shown to take place between one and two weeks before a steady-state is reached. Also, several models of nitrogen uptake from phytoplankton are tested; those most consistent with oligotrophic Gross Primary Production data result in lower far-field phytoplankton and zooplankton concentration maxima. Generally speaking, the magnitude and distribution of the far-field concentrations of marine microorganisms predicted in this study suggest that the proposed nutrient-enhancement scenarios do not resemble natural upwellings.

Keywords: deep-ocean water, nutrients, gross primary production, artificial upwelling.

INTRODUCTION

The biologically most productive oceanic regions correspond to upwellings where nutrient-rich deep water slowly moves upward. Through this process, typically generated by wind forces (Ekman surface drift) or by the divergence of ocean currents, the upwelled water is exposed to greater photosynthetically available solar radiation. In sharp contrast, vast areas of the tropical oceans are oligotrophic with strong and persistent density stratification (thermocline) that prevents abundant deep-water nutrients from reaching the surface. 'Artificial upwellings' essentially would 'bridge the gap' and bring nutrient-rich deep water

[a]Corresponding author: nihous@hawaii.edu

to the surface by anthropogenic means, e.g. with pipes and pumps. The purported goal embodied in this concept is the creation of open-ocean oases where increased productivity could sustain fisheries (Takahashi *et al.*, 1993). Before large-scale experimentation at sea is attempted, it is legitimate to wonder how effective engineering could be in 'turning the water column upside down' and in locally altering oligotrophic marine environments.

In a recent analysis, Nihous (2006) presented plume calculations corresponding to the near-field behavior of several 'artificial upwelling' concepts. These included estimates of the dilution and depth penetration of negatively buoyant discharges of deep water near the ocean surface. Such 'artificial upwellings' start with *downward* plumes that settle at a neutral-buoyancy depth in minutes; biological and diffusive processes are too slow to play a role in this early phase. Nihous (2006) further suggested that for initial Lagrangian releases Q^* exceeding about 15 m^3/s (e.g. *Figures 8* and *10*), even new production (photosynthetic) *potential* was unfavorable because of excessive plume settling depths.

The object of this study is to examine the interplay between diffusion and a few elementary biological processes in the far field, i.e. where initial buoyancy forces have vanished. Only Lagrangian releases will be considered, when there are no ambient currents (relatively to the discharge). These correspond to the 'drifting sea ranch' concept envisioned in Takahashi *et al.* (1993). A Lagrangian context allows the straightforward use of an oceanic diffusion model derived for drifting patches (instantaneous releases) and based on diffusion velocity[1].

[1] A continuous source may be viewed as a continuum of successive infinitesimal instantaneous terms. Diffusion velocity typically is defined as a function of the age of the patch or of distance to the patch center. Without ambient currents, the patch center for each infinitesimal source remains fixed and the diffusion coefficient can be unambiguously defined.

Before the far-field modeling approach is formulated and calculations performed in the next sections, the upwelling associated with the mesoscale cyclonic eddy *Haulani* described in Bidigare *et al.* (2003) and Vaillancourt *et al.* (2003) could be considered a benchmark -albeit of greater magnitude – for biological enhancement. Two months into its existence in 2000, in the lee of the Big Island of Hawaii, *Haulani* was characterized by an overall lifting of isotherms with a temperature depression exceeding 3°C at its center. Chlorophyll-a, representative of phytoplankton, and microheterotroph (e.g. zooplankton) concentrations integrated over the top 150 m showed enhancement factors of 1.3 and 2.2, respectively, inside the eddy.

MODELING APPROACH

The near field corresponds to the descending plume of negatively buoyant fluid injected at the ocean surface. As mixing with surrounding water occurs, plume dilution increases down to a depth where water density is the same inside and outside the plume. Such vertical stabilization results from density stratification in the upper ocean. Shortly before reaching this neutral-buoyancy depth, plume characteristics do not change much except for the centerline velocity u and the plume radius b, as illustrated in Figure 1. During plume descent, typically of the order of a few minutes, slower physical processes like diffusion and photosynthesis are negligible. They have to be taken into account, however, in what may be defined as the far field once buoyancy forces vanish. An interesting question, discussed for example in Zhang and Adams (1999), is the choice of an interface strategy between near and far fields. The far-field model selected here is extremely simplified, as shown in Figure 1, and rests on the assumption that vertical transport

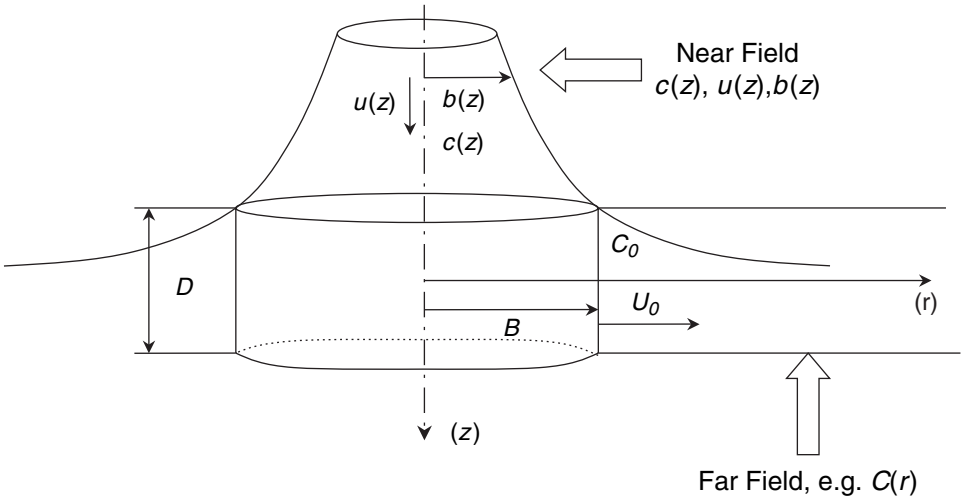

FIGURE 1
Schematic diagram showing the transition between near field and far field.

processes are negligible. Solutions are axisymmetric, like the near-field plume, and independent of the vertical coordinate z within a layer D centered across the neutral-buoyancy depth h_T. As a result, available flux continuity relationships from the near-field must be applied at the neutral-buoyancy depth h_T. This corresponds to interfacing *Method III* in Zhang and Adams (1999).

A general formulation of the far-field advection-diffusion problem in the absence of any sources and sinks is given below for $r \geq B$:

$$\frac{\partial C}{\partial t} + \frac{1}{r}\frac{\partial}{\partial r}(rUC) - \frac{1}{r}\frac{\partial}{\partial r}\left(r\tilde{D}\frac{\partial C}{\partial r}\right) = 0 \qquad (1)$$

Assuming that no additional mixing takes place in the far field, the velocity in Equation (1) simply is $U = (U_0 B)/r$. If horizontal oceanic diffusion is represented with a diffusion velocity P as $\tilde{D} = Pr$ (Joseph and Sendner, 1958), Equation (1) then becomes:

$$\frac{\partial C}{\partial t} + \frac{U_0 B}{r}\frac{\partial C}{\partial r} - \frac{1}{r}\frac{\partial}{\partial r}\left(Pr^2\frac{\partial C}{\partial r}\right) = 0 \qquad (2)$$

An order of magnitude for P is 0.1 to 1 cm/s. From the patch dispersion analysis of Schott *et al.* (1978), a value P = 0.25 cm/s is chosen for this study. Setting the time derivative to zero, the steady-state solution of Equation (2) subject to boundary conditions $C(B) = C_0$ and $C = C_\infty$ as r tends to infinity is found to be:

$$C = C_\infty + (C_0 - C_\infty)\frac{1 - \exp(-\frac{U_0 B}{Pr})}{1 - \exp(-\frac{U_0}{P})} \qquad (3)$$

In the Screening Information Data Set (SIDS) of the United Nations Environmental Program (2000), a recommended formula to estimate the concentration of discharged pollutants in the ocean is given. It corresponds to Equation (3) with $C_\infty = 0$ when B tends to zero (point source). In this case, U_0 tends to infinity while the product $U_0 B = Q/\varphi D$ is constant (for discharges along a coastline, the spreading angle φ is less than 2π).

In the absence of additional mixing in the transition region, flow continuity between the near and far fields is expressed as:

$$2U_0 BD = u(h_T)b(h_T)^2 \qquad (4)$$

Also, the flux continuity of any species represented by concentrations c and C in the near and far fields, respectively, can be written as:

$$2U_0BDC_0 - 2B^2DP\frac{\partial C}{\partial r}(B) = u(h_T)b(h_T)^2c(h_T) \quad (5)$$

Combining Equations (4) and (5) yields:

$$u(h_T)b(h_T)^2\{C_0 - c(h_T)\} = 2B^2DP\frac{\partial C}{\partial r}(B) \quad (6)$$

The far-field transition parameters B, D, U_0, and C_0 remain undetermined with two equations fewer than necessary. Without ambient flow in a linearly stratified fluid, the intrusion layer thickness is known to be of the order of the plume trap height (Wright *et al.*, 1982; Roberts *et al.*, 1989). Accordingly $D = h_T$ was selected. Next, it was verified from computational experiments that the choice of B does not affect the solution, since U_0B in Equation (2) is given from Equation (4), but only introduces a concentration discontinuity between near and far fields via Equation (6). In turn, this discontinuity only is a result of 'initiating' the far-field at $r = B$ away from the plume axis. Therefore, $B = 0$ was adopted as a baseline with no loss of generality; this choice also leads to concentration continuity between near and far fields, and eliminates the need to define different numerical domains for different plumes.

Table 1 includes relevant transition parameters and boundary conditions mostly from the plume calculations of Nihous (2006) using a 0.1 m vertical grid. Three surface releases of 400 m deep nutrient-rich seawater into an ambient water column representative of Station ALOHA (Hawaii Ocean Time-series) were considered: $Q^* = 1\,m^3/s$, $Q^* = 10\,m^3/s$ and $Q^* = 100\,m^3/s$.

The far-field calculations presented below involve the nitrogen concentrations of four

TABLE 1
Transition Parameters and Far-field Boundary Conditions.

	$Q^* = 1\,m^3/s$	$Q^* = 10\,m^3/s$	$Q^* = 100\,m^3/s$	NOTE
h_T(m)	62	89	139	Nihous (2006)
$b(h_T)$(m)	85.6	54.5	152	Nihous (2006)
$u(h_T)$(cm/s)	0.2	2.2	1.4	Nihous (2006)
θ(°C)	24	23	21	HOT data at h_T
$[N]_0$(nM)	391.3	906.6	1886.7	Nihous (2006)
$[N]_\infty$ (nM)	10	40	760	HOT data at h_T
$[A]_0$ (nM)	40	40	40	Assumed
$[A]_\infty$(nM)	40	40	40	Assumed
$[Phy]_0$ (nM)[a]	58.1	69.2	82.6	Nihous (2006)
$[Phy]_\infty$(nM)[a]	78.6	125.8	81.8	HOT data at h_T
$[Zoo]_0$ (nM)	85.8	194.2	94.9	Equilibrium at h_T
$[Zoo]_\infty$ (nM)	85.8	194.2	94.9	Equilibrium at h_T

[a] *Conversion from μg-Chl-a/l to nM-N based on a C:Chl-a mass ratio of 50 and a C:N molar ratio of 106/16*

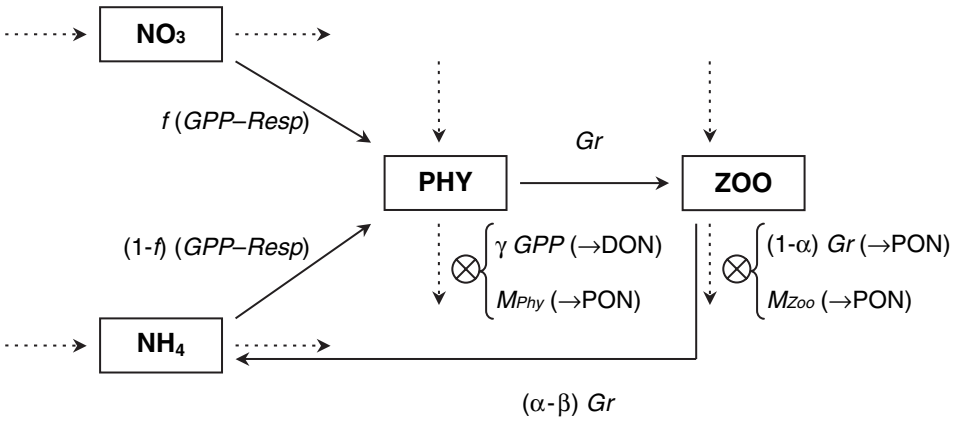

FIGURE 2
Schematic diagram of the simplified ecological model.

species: nitrate (plus nitrite) [*N*] considered to be a limiting nutrient for photosynthesis, ammonium [*A*] which recycles nitrogen for photosynthesis, phytoplankton [*Phy*] and herbivore zooplankton [*Zoo*]. To represent interactions among species, a simplified version of the ecological model of Kawamiya *et al.* (1995, 1997) is adopted as a baseline and shown in Figure 2. Because our advection-diffusion model is strictly horizontal, two computational compartments in the original formulation were omitted, giving rise to net 'losses' instead (symbol ⊗ in Figure 2): Particulate Organic Nitrogen (PON) which has the ability to sink[2], and Dissolved Organic Nitrogen (DON) which is affected 'upstream' by PON decomposition. Dotted arrows simply indicate advection and diffusion affecting all species. The nitrification of ammonium into nitrate is not included to partially offset missing ammonium sources from DON decomposition.

Mathematically, a system of four coupled partial differential equations has to be solved. These equations formally have the same left-hand-side as Equation (2), where the 'generic' concentration C represents each of the four unknowns, respectively, but with the following right-hand sides:

$$\text{For [N]} : -f(GPP - Resp) \\ -\{-f(GPP - Resp)\}_\infty$$

$$\text{For [A]} : -(1-f)(GPP - Resp) + (\alpha - \beta)Gr \\ -\{-(1-f)(GPP - Resp) + (\alpha - \beta)Gr\}_\infty$$

$$\text{For [Phy]} : (1-\gamma)GPP - Resp - Gr - M_{Phy} \\ -\{(1-\gamma)GPP - Resp - Gr - M_{Phy}\}_\infty$$

$$\text{For [Zoo]} : \beta\, Gr - M_{Zoo} - \{\beta\, Gr - M_{Zoo}\}_\infty$$

Far-field background values of the sources and sinks have been subtracted above to ensure that the system is in equilibrium when $C = C_\infty$ (no perturbation). Since the focus of this study is simply to highlight the relative effect of artificial deep seawater releases, such a procedure may be justifiable in the absence of a thorough calibration of the ecological model. Such a calibration would involve the vertically-resolved upper water column and include a determination of the mixed layer depth (Kawamiya *et al.*, 1995, 1997). This task certainly is desirable for the data collected at Station ALOHA,

[2] The potential effect of sinking particulate matter on *deeper* waters is not considered in this study, but is believed to be relatively small.

but it is beyond the scope of the present effort and is left for future consideration. On the other hand, the simplified, vertically independent model adopted here introduces net losses (sinks), as discussed earlier, even when $C = C_\infty$ (no perturbation); it is therefore necessary to adjust the sources and sinks in the right-hand-sides of the coupled partial differential equations. The proposed procedure may seem arbitrary but it straightforwardly achieves the desired goal of a well defined equilibrium.

The rate *GPP* at which phytoplankton concentration increases via photosynthetis is:

$$GPP = V_{max}\left\{\frac{[A]}{K_A+[A]}+\frac{[N]}{K_N+[N]} \times \exp(-\psi[A])\right\} A_{light}[Phy] \quad (7)$$

K_A and K_N are half-saturation constants. V_{max} is the maximum rate at ambient temperature θ. The factor $\exp(-\psi[A])$ represents the ammonium inhibition of nitrate uptake. With this nutrient assimilation formalism, the ratio f of new production over *GPP* is:

$$f = \frac{\frac{[N]}{K_N+[N]}\exp(-\psi[A])}{\frac{[N]}{K_N+[N]}\exp(-\psi[A])+\frac{[A]}{K_A+[A]}} \quad (8)$$

Light limitation averaged across the far-field layer is represented as:

$$A_{light} = \frac{\tilde{I}}{D}\int_{h_r-D/2}^{h_r+D/2} dz\, \mathbf{exp}\{-(\kappa+\kappa'[Phy])z\} \times \exp[1-\tilde{I}\,\exp\{-(\kappa+\kappa'[Phy])z\}] \quad (9)$$

where κ is the light extinction coefficient, κ' represents the effect of potential self-shading and $\tilde{I}$ is the ratio of surface photosynthetically available radiation (PAR) irradiance over optimum PAR irradiance.

Phytoplankton respiration is described by the simple linear relationship $Resp = R[Phy]$, while phytoplankton mortality and zooplankton mortality are represented by the quadratic expressions $M_{Phy} = R_{Phy}[Phy]^2$ and $M_{Zoo} = R_{Zoo}[Zoo]^2$, respectively. Grazing of phytoplankton by zooplankton only occurs when $[Phy]$ exceeds a threshold value $[Phy]^*$ and then, it may be represented by the function $Gr = Gr_{\max}[1-\exp\{\lambda([Phy]^*-[Phy])\}]\times[Zoo]$.

Table 2 provides a list of the baseline values used in the ecological model. Since ammonium concentrations have not been measured in the HOT program, but were deemed below standard detection levels of 50 nM, $[A]$ was assumed to have a background value of 40 nM. Likewise, the background concentration of zooplankton

TABLE 2
Baseline Values of Ecological Model Constants (Kawamiya *et al.*, 1995, 1997: KKYS).

$\tilde{I}^a$	1.35
$Gr_{\max}$	$0.4\times\exp(0.063\theta)$ day^{-1}
K_A	100 nM
K_N	30 nM
$[Phy]^*$	43 nM
R	$0.03\times\exp(0.0519\theta)$ day^{-1}
R_{Phy}	$2.81\times10^{-5}\times\exp(0.069\theta)$ nM^{-1} −day^{-1}
R_{Zoo}	$5.85\times10^{-5}\times\exp(0.0693\theta)$ nM^{-1} −day^{-1}
$V_{\max}$	$1\times\exp(0.063\,\theta)$ day^{-1}
α	0.7
β	0.3
γ	0.135
κ	0.035 m^{-1}
κ'	2.81×10^{-5} nM^{-1} − m^{-1}
λ	0.0014 nM^{-1}
ψ	0.0015 nM^{-1}

[a] *Value from Nihous (2006).*

was calculated from the equilibrium condition $\{\beta Gr - M_{Zoo}\}_\infty = 0$.

In the solution procedure, Dirichlet boundary conditions are applied, i.e. $C(B) = C_0$ and $C = C_\infty$ as r tends to infinity. In practice, the numerical domain can be extended to r_{max} in the radial direction until the solution becomes 'insensitive'. Values of r_{max} up to 10 and 20 km were tested.

RESULTS AND DISCUSSION

Steady-state Solutions

First, steady-state solutions were sought by setting time derivatives to zero in the partial differential equations. Figures 3 to 6 show numerical results for the four variables as functions of r in the two cases $Q^* = 1\text{m}^3/\text{s}$ and $Q^* = 10\,\text{m}^3/\text{s}$. With the larger plume $Q^* = 100\,\text{m}^3/\text{s}$, negligible biological enhancement occurred due to excessive depths and a corresponding lack of photosynthetically available radiation. In Figure 3, the value of $[N]$ according to Equation (3) is also plotted to give a measure of the relative impact of biological processes.

As can be seen in Figure 3, $[N]$ drops within 10% of the background value at a radial distance of less than 500 m for the smaller release; a commensurate drop takes place about 2 km away for the larger release. Nitrate consumption via photosynthesis sustains a localized net increase of phytoplankton concentrations; Figure 4 shows maxima of $[Phy]$ at about 145 m and 500 m for $Q^* = 1\,\text{m}^3/\text{s}$ and $Q^* = 10\,\text{m}^3/\text{s}$, respectively. These radial distances correspond

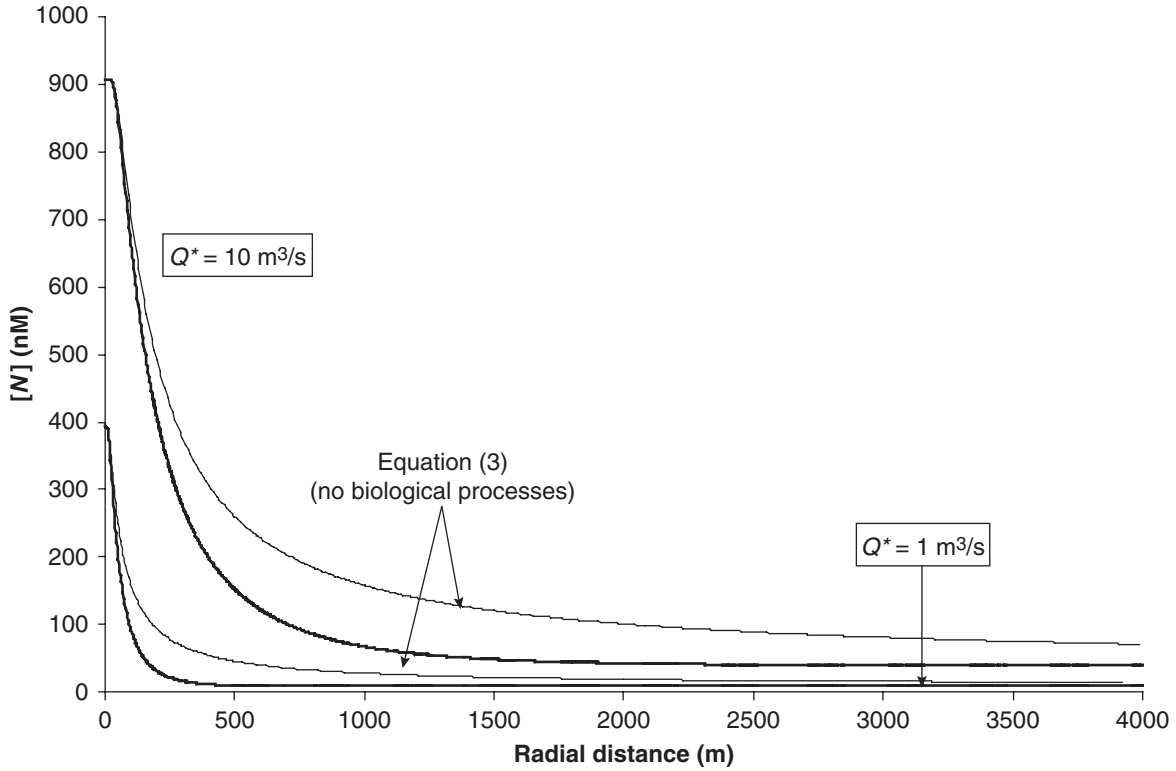

FIGURE 3
Calculated far-field nitrate concentration as a function of radial coordinate.

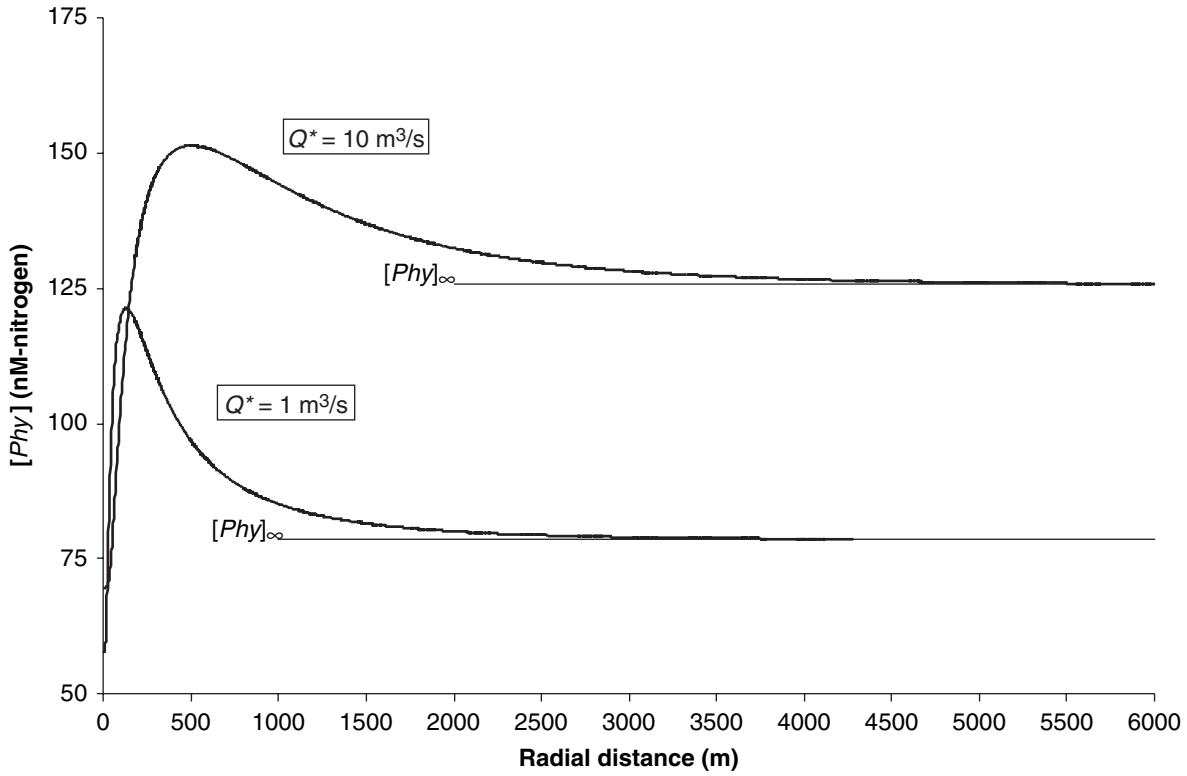

FIGURE 4
Calculated far-field phytoplankton concentration as a function of radial coordinate.

to nitrate concentrations of the order of 15% of $[N]_0$. Figure 5 displays a localized growth of the herbivore zooplankton stock through grazing. Maxima of $[Zoo]$ are broad and approximately start where phytoplankton concentrations peak.

So far, far-field features have seemed quite similar for the two releases. Yet, Figure 6 suggests that there are some substantial differences as well since ammonia levels increase in one case while they drop in the other. In order to interpret this result, 'excess-nitrogen' integrals $I_C = 2\pi D \int_B^{r_{\max}} r\{C - C_\infty\}dr$ were computed over the numerical domain, where C represents any of the four variables. This allowed a determination of 'excess-nitrogen' fractions $\xi_C = I_C/(I_N + I_A + I_{Phy} + I_{Zoo})$ shown in Table 3. For $Q^* = 1\,\mathrm{m}^3/\mathrm{s}$, biological utilization of excess inorganic nitrogen is practically complete (in a sense, it exceeds 100% since the net ammonium drawdown shown in Figure 6 results in a negative value of ξ_A). For $Q^* = 10\,\mathrm{m}^3/\mathrm{s}$, about 55 % of excess nitrogen only is in organic form. Biological processes in general are not fast enough to utilize the large amount of excess nutrients before they diffuse away. Also, photosynthesis is less competitive against grazing pressure, which results in a relatively greater buildup of herbivore concentrations and in a net increase in ammonium levels ($\xi_A > 0$) from the excretion flux $(\alpha - \beta)Gr$.

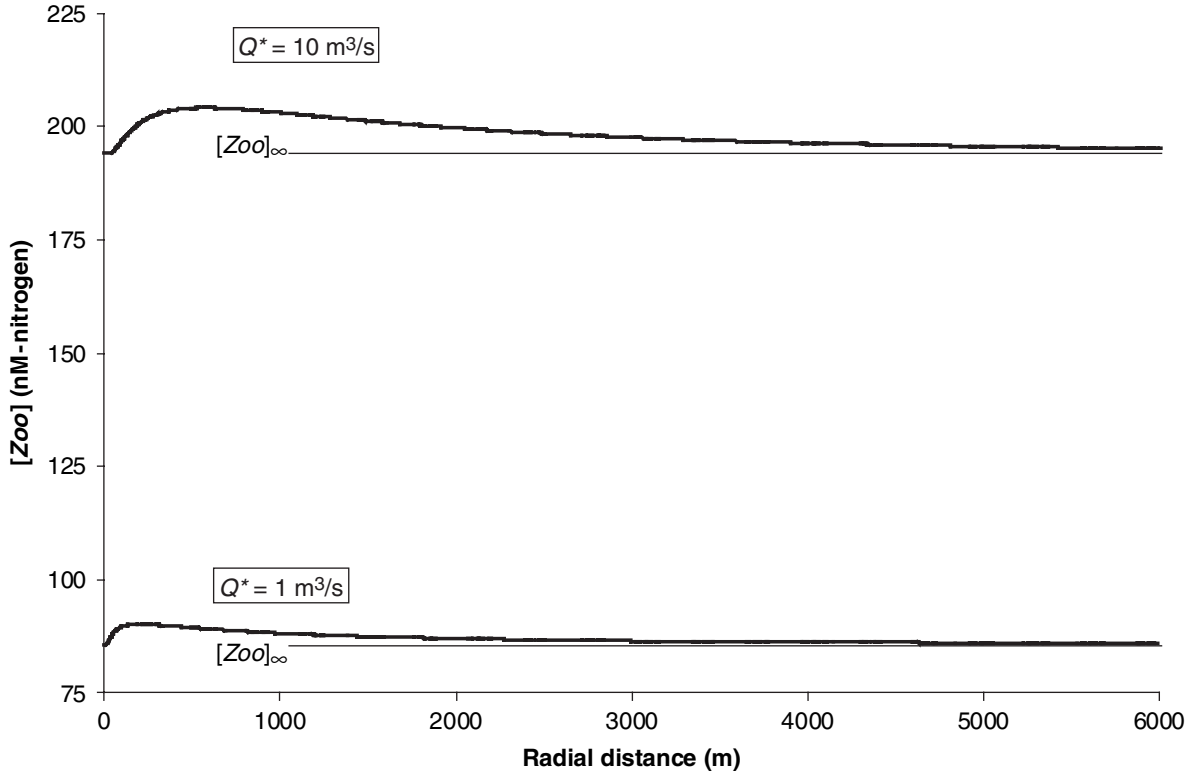

FIGURE 5
Calculated far-field zooplankton concentration as a function of radial coordinate.

Time Scales

Of substantial interest is the time it would take for the steady-state solution to be reached. A simple heuristic argument allows a useful estimation without performing time-domain calculations (nonzero partial derivatives with respect to time). The convective 'excess-nitrogen' flux into the far field (at $r = B$) essentially is responsible for the buildup of excess nitrogen in the computational domain. An estimate τ of the time to reach steady state therefore is:

$$\tau = \frac{I_N + I_A + I_{Phy} + I_{Zoo}}{2\pi B U_0 \{[N]_0 - [N]_\infty + [Phy]_0 - [Phy]_\infty\}} \quad (10)$$

In this expression, the denominator does not include contributions from ammonium and zooplankton because near-field and background concentrations of these species have been assumed to be equal.

Applying Equation (10) to the two cases $Q^* = 1\,\mathrm{m}^3/\mathrm{s}$ and $Q^* = 10\,\mathrm{m}^3/\mathrm{s}$ yields respective values of τ equal to 7.6 days and 7.9 days.

In turn, this 'rule of thumb' can be tested if the time-domain equations are solved. The initial condition is specified by background values through the computational domain. On the basis of such calculations, Figure 7 shows the relative convergence of transient phytoplankton and zooplankton concentration maxima to their steady-state values as a function

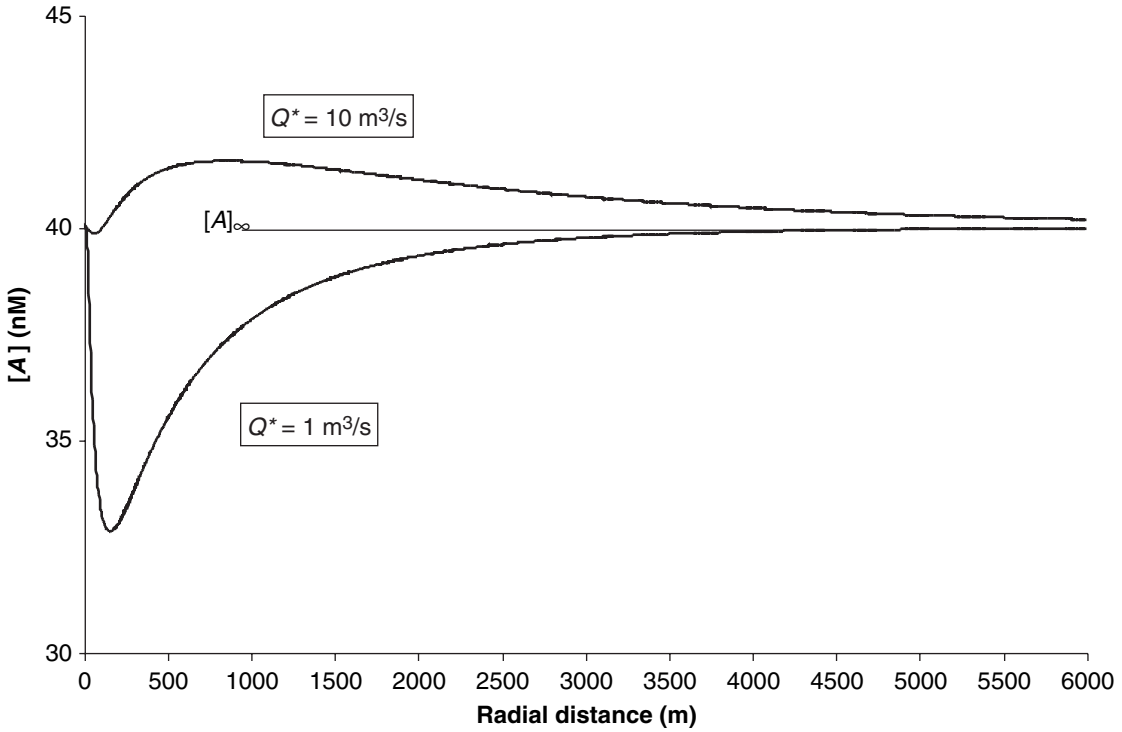

FIGURE 6
Calculated far-field ammonium concentration as a function of radial coordinate.

TABLE 3
Selected 'excess-nitrogen' parameters for three AU releases and different GPP models.[a]

	$Q^* = 1\,m^3/s$	$Q^* = 10\,m^3/s$	$Q^* = 100\,m^3/s$	KKYS Mod # 1	KKYS Mod # 2	HHI
ξ_{Phy}	0.42	0.19	< 0.01	0.27	0.18	0.28
ξ_{Zoo}	0.68	0.37	< 0.01	0.38	0.23	0.40
ξ_N	0.03	0.35	> 0.99	0.55	0.68	0.74
ξ_A	−0.13	0.08	< 0.01	−0.20	−0.08	−0.41
I_{Phy} (mol)	4.86	21.94	11.14	5.06	4.77	5.02
I_{Zoo} (mol)	7.73	42.22	10.79	7.10	6.09	7.18

[a] *The different models of Gross Primary Production are tested with* $Q^* = 1\,m^3/s$.

of time. It turns out that the time scale of net phytoplankton growth is well approximated by Equation (10). Zooplankton concentrations, however, converge more slowly and require about 12 days to approach their steady-state level; such a delayed response should not be too surprising from secondary growth processes.

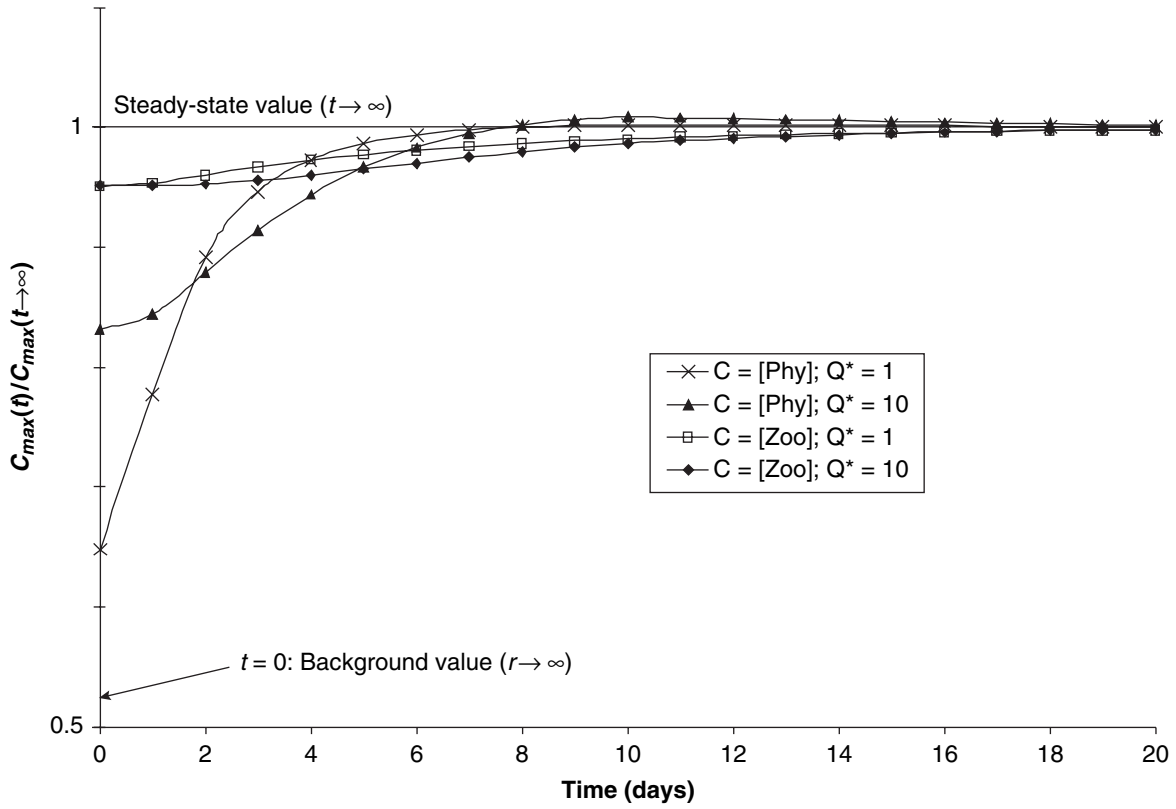

FIGURE 7
Ratio of maximum far-field concentration over its steady-state value as a function of time.

Nitrogen Uptake Models

In this study, the baseline model for GPP was borrowed from Kawamiya *et al.* (1995, 1997); its nitrogen uptake function, $V_{max}\{([A]/(K_A + [A])) + ([N]/(K_N + [N]))\exp(-\psi[A])\}$, is hence designated as KKYS. One of the parametric modifications proposed by the authors in their latter work was to drop K_N from 3000 nM to 30 nM in order to better represent phytoplankton communities adapted to oligotrophic conditions (e.g. in tropical oceans). This is consistent with the results of incubation experiments performed by Harrison *et al.* (1996). These researchers proposed a different nitrogen uptake function in Equation (7), namely $[V_A([A]/(K_A + [A])) + V_N([N]/(K_N + [N]))(1 - (I_m[A]/(K_i + [A])))]$. In this formalism, labeled HHI, there are separate maximum uptake rates for ammonium and nitrate (at a given temperature); also, the factor $(1 - (I_m[A]/(K_i + [A])))$ representing the ammonium inhibition of nitrate uptake depends on two constants I_m and K_i.

Nihous (2006) calibrated Equation (7) with the HHI nitrogen uptake function by using Gross Primary Production data averaged over the first 133 HOT cruises. An additional constraint was the average flux of Particulate Organic Nitrogen at 150 m, equal to 4.2 mg-N/m^2-day, which is a measure of integrated new production in the upper 150 m.

Trying to repeat this procedure with the KKYS baseline model did not succeed well. Generally speaking, it yielded *f* ratios that are far too high for the oligotrophic environment of the North Pacific Subtropical Gyre. This may seem surprising since the *f* ratios obtained by Kawamiya *et al.* (1997) for the Bermuda data set (BATS) are low and compatible with observations. The apparent discrepancy may be due to some of the simplifications adopted here (e.g. constant background ammonium concentrations), but it would be difficult to investigate without conducting a calibration of the *complete* ecological model for the upper water column at Station ALOHA. Meanwhile, two modified versions of the KKYS nitrogen-uptake model (designated KKYS Mod # 1 and KKYS Mod # 2) were considered in order to bring new production down to the observed low levels. This was accomplished by substantially raising the ammonium inhibition factor ψ (Mod # 1) or the nitrate half-saturation constant K_N (Mod # 2), as summarized in Table 4. The fit of the modified models to Gross Primary Production data can be seen in Figure 8. The fact that widely different parametric choices all appear satisfactory highlights the need for additional constraints, and also calls for caution.

Figures 9 and 10 show calculated far-field phytoplankton and zooplankton concentrations with the alternative nitrogen uptake models and $Q^* = 1\ \mathrm{m}^3/\mathrm{s}$. In spite of different parametrizations, all results seem reasonably close to one another; the local maxima are sharply reduced from their baseline values of about 122 nM (Figure 4) and 90 nM (Figure 5). Yet, less perceptible differences at high radial coordinates result in only small changes in the 'excess-nitrogen' integrals I_{Phy} and I_{Zoo}, as seen in Table 3. 'Excess-nitrogen' fractions are substantially altered, however, with the bulk of excess nitrogen in the form of unutilized nitrate. The KKYS Mod #1 and HHI alternative nitrogen uptake models strongly favor the cycling of ammonium over new production; as a result, Gross Primary Production is 'triggered' by the large nitrate influx, but proceeds largely by

TABLE 4
Constants in Alternative GPP Models.

	KKYS Mod # 1[a]	KKYS Mod # 2[a]	HHI[b]
I_m	N/A	N/A	0.60
K_A	28 nM	75 nM	10 nM
K_i	N/A	N/A	60 nM
K_N	Baseline	1250 nM	Baseline
V_{max}	$0.7 \times \exp(0.055\,\theta)\ \mathrm{day}^{-1}$	Baseline	N/A
V_A	N/A	N/A	$2 \times \exp\{0.063(\theta - 24.91)\}\ \mathrm{day}^{-1}$
V_N	N/A	N/A	$0.4 \times \exp\{0.063(\theta - 24.91)\}\ \mathrm{day}^{-1}$
ψ	$0.0552\ \mathrm{nM}^{-1}$	Baseline	N/A

[a] *Only parameters with values different from baseline (Table 2) are shown.*
[b] *Values of the constants from Nihous (2006) to fit average HOT data (first 133 cruises).*

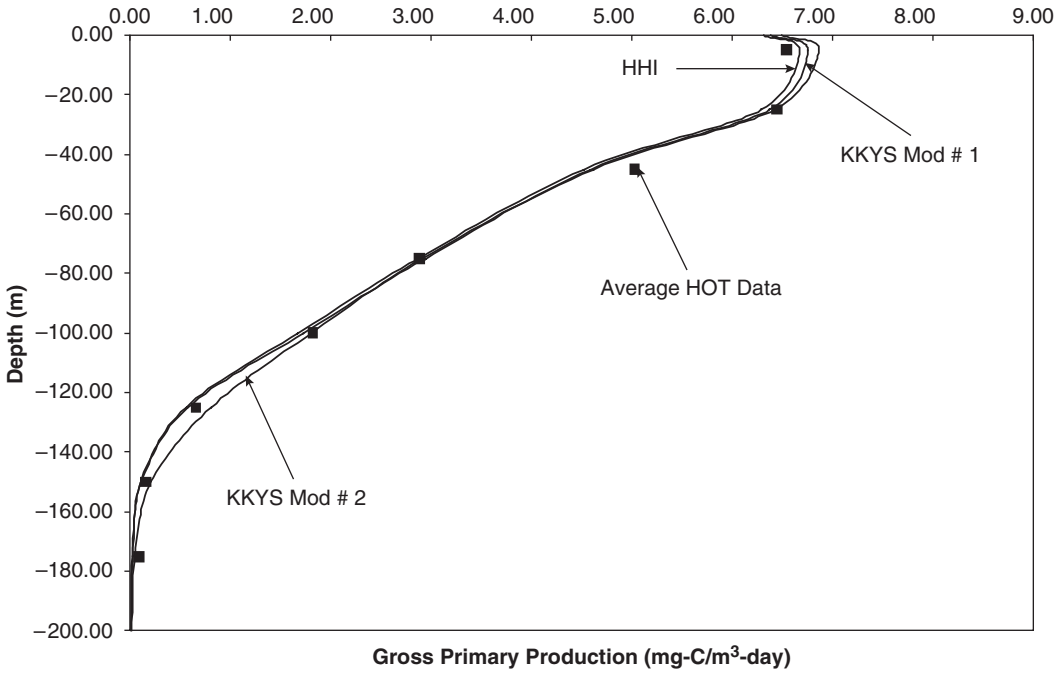

FIGURE 8
Calculated GPP profiles with several nitrogen uptake models and average HOT data ("Light 12", Cruises 1-133).

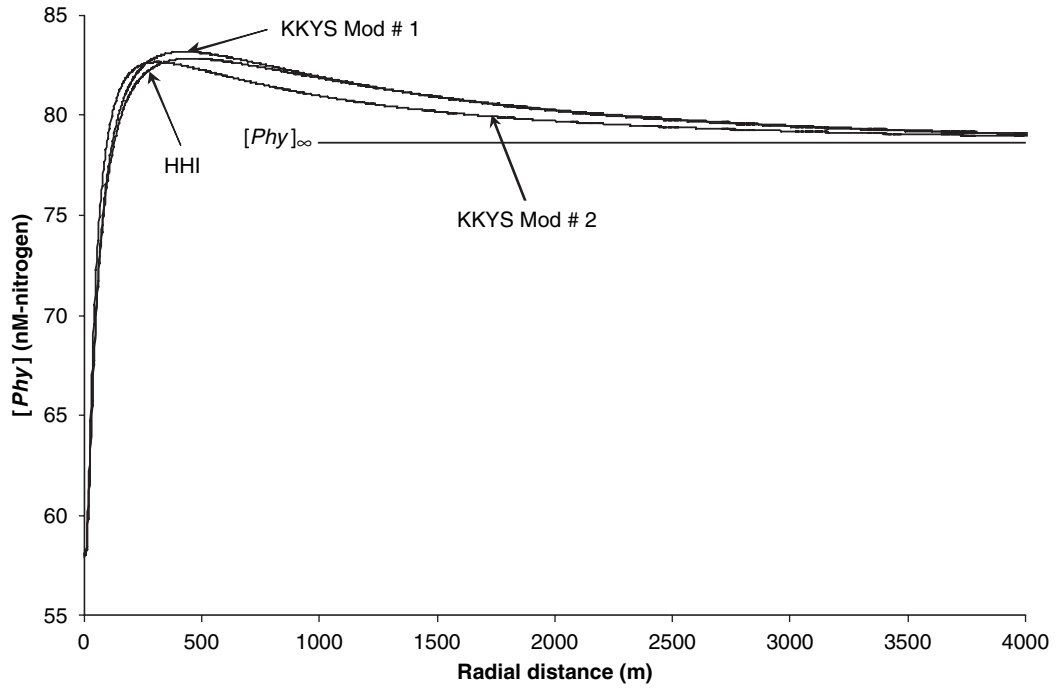

FIGURE 9
Calculated far-field phytoplankton concentration with alternative nitrogen uptake models (Q^*= 1 m^3/s).

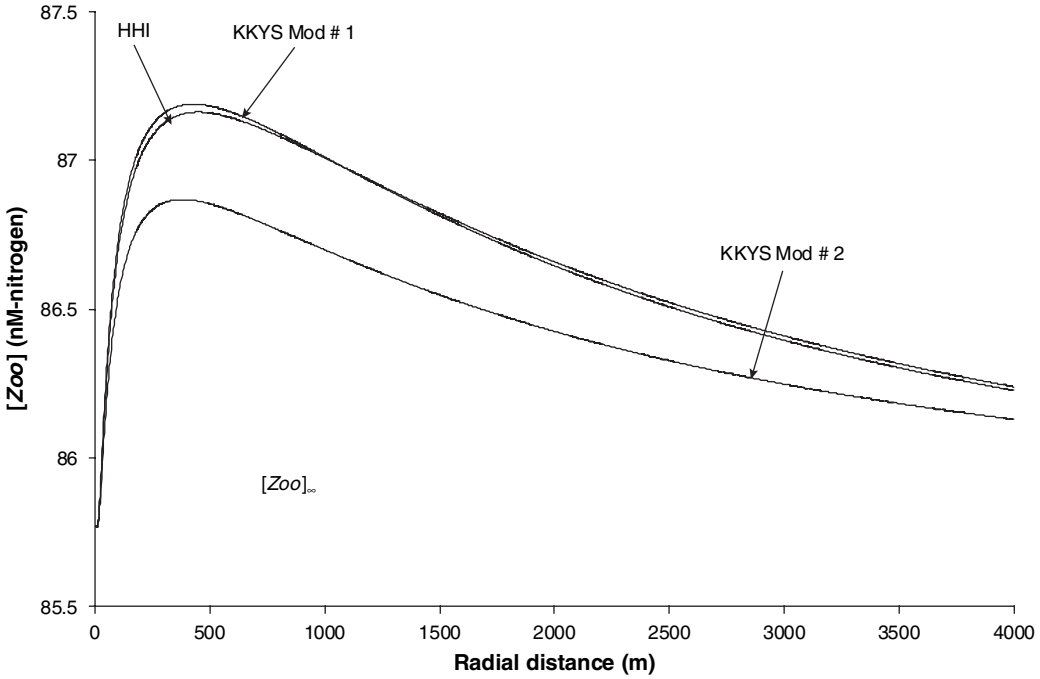

FIGURE 10
Calculated far-field zooplankton concentration with alternative nitrogen uptake models (Q^*= 1 m^3/s).

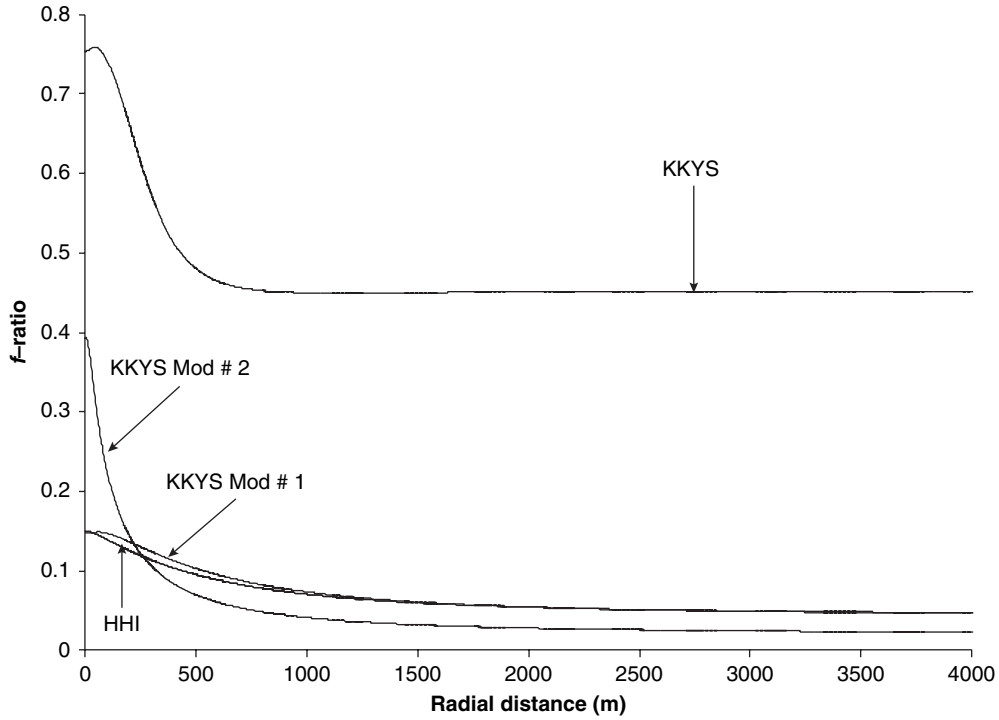

FIGURE 11
Calculated far-field *f*-ratio for all nitrogen uptake models (Q^*= 1 m^3/s).

consuming ammonium. In the KKYS Mod # 2 case, the high value of K_N prevents nitrate utilization from reaching saturation, but the *f*-ratio still shows a strong local buildup, as seen in Figure 11.

CONCLUSIONS

A model of the evolution of axisymmetric releases of deep nutrient-rich seawater near the ocean surface was developed when buoyancy forces vanish (far field). Cases under consideration correspond to the absence of relative currents between the release point and the ocean water column. The proposed algorithm essentially extended previous plume calculations (near field) into a spatial and temporal framework where slow diffusive and biological processes become important.

It was shown that large releases corresponding to Q^* of the order $100\,m^3/s$ failed to trigger biological enhancement; this was anticipated from the near-field analysis (Nihous, 2006) on the basis of excessive neutral-buoyancy depths and a corresponding lack of photosynthetically available radiation. For moderate releases, phytoplankton and zooplankton growth would be promoted within a narrow vertical layer extending a few kilometers radially, depending on Q^*. With Q^* of the order $1\,m^3/s$ and shallower settling depths, a more complete far-field conversion of excess nutrients into organic matter was achieved. With Q^* of the order $10\,m^3/s$ and deeper neutral-buoyancy depths, weaker photosynthesis could not thoroughly process the larger amount of excess nutrients; grazing pressure also seemed to become relatively stronger.

Changes in the concentrations of phytoplankton and zooplankton were shown to take place between one and two weeks before steady-state values were reached, with primary growth processes being faster.

Because the baseline formalism of nitrogen uptake from phytoplankton was shown to over-predict new production in oligotrophic conditions (e.g. at Station ALOHA, North Pacific Subtropical Gyre), different nitrogen-uptake models were tested. Those most able to reproduce Gross Primary Production data at Station ALOHA generally led to relatively lower far-field phytoplankton and zooplankton concentration maxima. Integrating excess concentrations over the computational domain, however, showed that these potentially more realistic nitrogen uptake models only had a modest effect on phytoplankton excess biomass; zooplankton excess biomass dropped more consistently. A better understanding of nitrogen cycling by phytoplankton seems warranted in nutrient-depleted oceanic regions.

Generally speaking, the magnitude and distribution of the far-field concentrations of marine microorganisms predicted in this study may not justify the proposed nutrient-enhancement scenarios as 'artificial upwellings'. The failure of the scenario with $Q^* = 100\,m^3/s$ to initiate biological enhancement reflects fundamental physical dissimilarities between natural upwellings and artificial near-surface releases of deep nutrient-rich seawater: in the former case, the entire water column is uplifted toward more abundant photosynthetically available radiation, while in the latter case, the near field is a fast moving *downwelling* of the released water followed by slow lateral dispersion at neutral-buoyancy depth in the far field. With excessive values of Q^*, the near field simply extends too far down for net photosynthetic enhancement. This situation would be altered by the presence of cross currents and such cases are under investigation.

Nomenclature

A_{light}	light factor in Equation (7), described in Equation (9)
$[A]$	ammonium concentration (M)
b	plume radius as a function of vertical coordinate (m)
B	far-field transition radius (m)
c	plume concentration as a function of vertical coordinate (M)
C	far-field concentration as a function of radial coordinate and time (M)
C_{max}	maximum far-field concentration as a function of time (M-nitrogen)
D	far-field layer thickness (m)
$\tilde{D}$	far-field diffusion coefficient as a function of radial coordinate (m^2/s)
f	ratio of phytoplankton new production over Gross Primary Production
GPP	phytoplankton Gross Primary Production (M-nitrogen/day)
Gr	grazing function (M-nitrogen/day)
Gr_{max}	maximum grazing rate at ambient temperature (day^{-1})
h_T	plume neutral-buoyancy (stabilization) depth (m)
I	'excess-nitrogen' integral (mol)
$\tilde{I}$	ratio of surface photosynthetically available radiation (PAR) irradiance over optimum PAR irradiance
I_m	proportionality constant for the ammonium inhibition of nitrate uptake in the model of Harrison *et al.* (1996)
K	half-saturation constant (M)
K_i	half-saturation constant for the ammonium inhibition of nitrate uptake in the model of Harrison *et al.* (1996) (M)
M	mortality (M-nitrogen/day)
$[N]$	nitrate (plus nitrite) concentration (M)
P	diffusion velocity (m/s)
$[Phy]$	phytoplankton concentration (M-nitrogen)
$[Phy]^*$	threshold phytoplankton concentration for grazing (M-nitrogen)
Q	volumetric discharge (m^3/s)
Q^*	volumetric surface discharge of deep nutrient-rich seawater (m^3/s)
r	radial coordinate (m)
r_{max}	maximum radial coordinate in computational domain (m)
R	phytoplankton respiration rate at ambient temperature (day^{-1})
R_{Phy}	phytoplankton mortality rate at ambient temperature ($M^{-1} - day^{-1}$)
R_{Zoo}	zooplankton mortality rate at ambient temperature ($M^{-1} - day^{-1}$)
$Resp$	phytoplankton respiration (M-nitrogen/day)

t	time (s)
u	plume vertical velocity as a function of vertical coordinate (m/s)
U	far-field horizontal velocity as a function of radial coordinate (m/s)
V_{max}	maximum photosynthetic rate at ambient temperature (day^{-1})
z	vertical coordinate (m)
$[Zoo]$	zooplankton concentration (M-nitrogen)

Greek letters

α	assimilation efficiency of zooplankton
β	growth efficiency of zooplankton
γ	ratio of extra cellular excretion over Gross Primary Production
κ	light extinction coefficient (m^{-1})
κ'	self-shading light extinction coefficient ($M^{-1} - m^{-1}$)
λ	Ivlev constant (M^{-1})
φ	spreading angle of discharge (rad)
ψ	ammonium inhibition factor (M^{-1})
θ	temperature ($^{\circ}C$)
τ	estimated time to reach steady state (s)
ξ	'excess-nitrogen' fraction

Subscripts

A	ammonium NH_4
N	nitrate NO_3(plus nitrite NO_2)
Phy	phytoplankton
Zoo	zooplankton
0	far-field transition boundary value
∞	far-field background value

REFERENCES

Bidigare, R. R., Benitez-Nelson, C., Leonard, C. L., Quay, P. D., Parsons, M. L., Foley, D. G. and Seki, M. P. (2003). "Influence of a cyclonic eddy on microheterotroph biomass and carbon export in the lee of Hawaii," *Geophysical Research Letters*, **30**(6), 4 pages.

Harrison, W. G., Harris, L. R. and Irwin, B. D. (1996). "The kinetics of nitrogen utilization in the oceanic mixed layer: Nitrate and ammonium interactions at nanomolar concentrations," *Limnology and Oceanography*, **41**(1), 16–32.

Joseph, J. and Sendner, H. (1958). "The horizontal diffusion in the Ocean," *Deutsche Hydrographische Zeitschrift,* **11**, 49–77.

Kawamiya, M., Kishi, M. J., Yamanaka, Y. and Suginohara, M. (1995). "An ecological-physical coupled model applied to Station Papa," *Journal of Oceanography*, **51**, 635–664.

Kawamiya, M., Kishi, M. J., Yamanaka, Y. and Suginohara, M. (1997). "Obtaining reasonable results in different oceanic regimes with the same ecological-physical coupled model," *Journal of Oceanography*, **53**, 397–402.

Nihous, G. C. (2006). "Near-field evaluation of Artificial Upwelling concepts for open-ocean oligotrophic conditions," *Journal of Marine Environmental Engineering*, **8**(3), 225–246.

Roberts, P. J. W., Snyder, W. H., and Baumgartner, D. J. (1989). "Ocean outfalls: I: Submerged wastefield formation. II: Spatial evolution of submerged wastefield. III: Effect of diffuser design on submerged wastefield," *Journal of Hydraulic Engineering*, **115**, 1–70.

Schott, F., Ehlers, M., Hubrich, L., and Quadfasel, D. (1978). "Small-Scale Diffusion Experiments in the Baltic Surface-Mixed Layer under Different Weather Conditions," *Deutsche Hydrographische Zeitschrift,* **6**, ISSN 0012-0308, 195–215 (also at http://www.baltic.vtt.fi/pdfs/dhz316schott.pdf)

Screening Information Data Sets of the Organisation for Economic Co-operation and Development (OECD SIDS) (2000). "Example of Diacetone Alcohol, Case 123-42-2," United Nations Environmental Program (UNEP) Publications, http://www.chem.unep.ch/irptc/sids/OECDSIDS/123422.pdf., 138–165.

Takahashi, P. K., McKinley, K. R., Phillips, V. D., Magaard, L. and Koske, P. (1993). "Marine macrobiotechnology systems," *Journal of Marine Biotechnology*, **1**, 9–15.

Vaillancourt, R. D., Marra, J., Seki, M. P., Parsons, M. L. and Bidigare, R. R. (2003). "Impact of a cyclonic eddy on phytoplankton community structure and photosynthetic competency in the subtropical North Pacific Ocean," *Deep Sea Research I*, **50**, 829–847.

Wright, S. J., Wong, D. R., Zimmerman, K. E., and Wallace, R. B. (1982). "Outfall Diffuser Behavior in Stratified Ambient Fluid," *ASCE Journal of the Hydraulics Division*, **108**(4), 483–501.

Zhang, X. Y., and Adams, E. E. (1999). "Prediction of Near Field Plume Characteristics Using Far Field Circulation Model," *Journal of Hydraulic Engineering*, **125**(3), 233–241.